Three-dimensional ballistic deposition at oblique incidence

Paul Meakin*
Central Research and Development, The Du Pont Company, Wilmington, Delaware 19880-0356

Joachim Krug†
IBM Thomas J. Watson Research Center, P.O. Box 218, Yorktown Heights, New York 10598

(Received 4 May 1992)

A simple lattice model has been used to investigate (2+1)-dimensional ballistic deposition for angles of incidence θ in the range $0° \leq \theta < 90°$. In the oblique-incidence limit ($\theta \to 90°$) a pattern of overlapping scales inclined at an angle of about 37.5° is formed. The individual scales can be characterized in terms of their characteristic length, width, and thickness which grow algebraically with increasing scale size. All of the scaling exponents characterizing the growing surface can be obtained from exponents $\sigma_x = 1/3$ and $\sigma_y = 2/3$ that describe the growth of the correlation lengths ξ_x and ξ_y parallel and perpendicular to the plane of incidence. The scaling properties of the columnar patterns can be understood in terms of the (1+1)-dimensional dynamics of the leading edges of the advancing scales. An anisotropic generalization of the finite-size scaling form of Family and Vicsek [J. Phys. A **18**, L75 (1985)] is proposed and its validity is demonstrated for ballistic deposition at near-grazing incidence.

PACS number(s): 81.15.Ef, 05.40.+j, 68.55.Jk, 68.35.Bs

I. INTRODUCTION

The formation of random rough surfaces under both equilibrium and nonequilibrium conditions has been an area of considerable scientific interest for several decades. In recent years this interest has intensified with the realization that rough surfaces formed under a broad range of conditions exhibit a variety of fractal [1] scaling properties. Interest has also been stimulated by substantial progress towards a theoretical understanding of the growth of rough surfaces under nonequilibrium conditions. Much of this progress is described in a recent review [2] but this is a rapidly developing area.

Computer simulations have played an important role at all stages of development. Vold [3–5] pioneered the application of simple ballistic deposition models in which particles are added, one at a time, to a growing deposit via linear or ballistic trajectories to study sedimentation processes. During the 1970s several simple ballistic deposition models were developed [6–9] to obtain a better understanding of vapor deposition onto cold substrates. A variety of experimental studies [10–14] showed that as the angle of incidence (θ) was changed from 0° (normal incidence) to $\simeq 90°$ (grazing incidence) the deposit structure changed from a porous structure that is uniform on all but very small length scales to a "columnar" structure in which the columns are well separated and have a characteristic angle of inclination ϕ that is different from θ.

More recently interest has become focused on the universal affine scaling structure of surfaces generated by the ballistic deposition model, the Eden model [15], and a variety of related nonequilibrium growth models [16]. In the standard models the surface is smooth at the start of a simulation (time $t=0$). Under these circumstances the evolution of the surface can be described in terms of the correlation lengths $\xi_\perp$ and $\xi_\parallel$ that characterize the magnitude of the surface roughness and the lateral distance over which correlations in the surface height fluctuations persist. These correlations grow algebraically with increasing time or deposit thickness

$$\xi_\perp \sim t^\beta , \tag{1a}$$

$$\xi_\parallel \sim t^{1/z} . \tag{1b}$$

On length scales shorter than these correlation lengths (but larger than the particle size or lattice unit used in the simulations) these rough surfaces can be described as self-affine fractals [1,17] and the correlation lengths are related by

$$\xi_\perp \sim \xi_\parallel^\zeta , \tag{2}$$

where the exponent $\zeta = \beta z$ is equivalent to the Hurst exponent [1,16] of the self-affine surface. The exponent ζ is frequently referred to as the wandering or roughness exponent.

Computer simulations are frequently carried out in narrow channels of width L with periodic boundary conditions in the lateral direction. In the case of a (1+1)-dimensional lattice model the surface width ξ (a measure of the correlation length $\xi_\perp$) is then given by

$$\xi(L,\bar{h})^2 = \frac{1}{L}\sum_{i=1}^{L}(h_i - \bar{h})^2 , \tag{3}$$

where $\bar{h}$ is the mean surface height and h_i is the height of the surface in the ith column of the lattice. The dependence of the surface width on L and $\bar{h}$ can be summarized by the simple scaling form [18]

$$\xi(L,\bar{h}) = L^\zeta f(\bar{h}/L^z) , \tag{4}$$

where $f(x)$ has a constant value ($\xi \sim L^\zeta$) in the station-

ary limit ($x \gg 1$). At early times ($x \ll 1$) $f(x) \sim x^{\beta}$ so that $\xi \sim \bar{h}^{\beta}$. The realization that simulation results obtained using both the ballistic deposition [18] and Eden [19] models could be described in terms of the scaling form given in Eq. (4) with similar values for the exponents ζ and z provided additional impetus to the growing interest in surface growth models.

The continuum equation of Kardar, Parisi, and Zhang [20] (KPZ) provides a firm theoretical foundation for these simulation results. While this equation was originally introduced in the context of the Eden growth process, it describes the ballistic deposition model (and many other surface growth models) equally well.

At non-normal angles of incidence the scaling form described above survives for the $(1+1)$-dimensional ballistic deposition model but the scaling exponents appear to change continuously with the angle of incidence [21,22]. At grazing incidence $\zeta = 1$ and $z = 2$. These exponents can be understood in terms of a mapping of the column growth and shadowing onto a diffusion-limited particle coalescence model [22]. At intermediate angles of incidence a satisfactory theoretical understanding is still lacking.

The scaling form described above also provides a good description of the evolving surface roughness associated with $(2+1)$-dimensional ballistic deposition models at normal incidence. However, the characteristic exponents ζ and z have values that are different from their $(1+1)$-dimensional values. It can be shown that the exponents ζ and z satisfy the scaling relation [2,23,24]

$$\zeta + z = 2 \tag{5}$$

(a simple derivation can be found in Ref. [2]).

At non-normal incidence there is no longer a single correlation length ($\xi_{\parallel}$) in the direction parallel to the surface. The projection of the deposition beam onto the substrate plane singles out a direction (the x direction in Fig. 1) and a more general, anisotropic scaling form involving two correlation lengths ξ_x and ξ_y is required. We [25] have previously published a preliminary account of our work on $(2+1)$-dimensional ballistic deposition near to grazing incidence. There it was shown that the correlation lengths ξ_x and ξ_y grow with different powers of the time

$$\xi_x \sim t^{\sigma_x} , \tag{6a}$$

$$\xi_y \sim t^{\sigma_y} , \tag{6b}$$

where $\sigma_x = 1/3$ and $\sigma_y = 2/3$. All scaling exponents characterizing the growing surface and the columnar structure can be derived from σ_x and σ_y. In the present paper we give a detailed account of our numerical work, including results at intermediate angles of incidence. Moreover, we present an anisotropic generalization of the finite-size scaling form (4) and demonstrate its validity for three-dimensional ballistic deposition at near-grazing incidence.

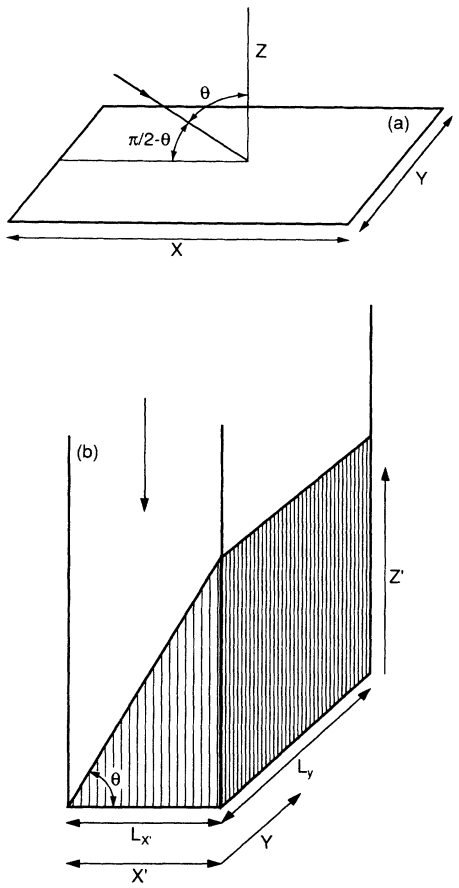

FIG. 1. Coordinate systems used in this work. (a) shows ballistic deposition at oblique incidence. The arrow indicates the direction of incidence and θ is the angle of incidence. (b) shows the coordinate system used in the simulations. The x', y, and z' coordinates are oriented along the axes of a cubic lattice. The surface of the shaded region is filled at time $t = 0$ to represent an inclined substrate.

II. COMPUTER SIMULATIONS

All of the computer simulations were carried out on cubic lattices with a cross section of $L_x \times L_y$ lattice units. To represent deposition onto a planar substrate with an angle of incidence of θ we simulate the ballistic deposition of particles occupying individual lattice sites via vertical trajectories onto an inclined substrate (Fig. 1). In the model used in this work "active zone" sites (sites into which growth may occur) are selected at random, with equal probabilities to represent the growth of a rough surface. At all stages in the simulation there is one active zone site for each column of the lattice. At the start of a simulation (time $t = 0$) the height of the active zone site in the column with lateral coordinates (i,j) is equal to $i \tan(\theta)$, truncated to the nearest smaller integer. If an active zone site at (i,j) is selected at random then the site at $h_a(i,j)$ is filled and the height of the active zone site associated with the column at (i,j) is increased by 1,

$$h_a'(i,j) = h_a(i,j) + 1 . \tag{7}$$

The heights of the active zone sites in the neighboring columns at positions $(i,j-1)$, $(i,j+1)$, $(i-1,j)$, and $(i+1,j)$ are then examined and increased to $h_a(i,j)$ (the height of the newly occupied surface site) if their heights are smaller than $h_a(i,j)$. The simulation of the ballistic deposition process consists of a sequence of events in which active zone sites (or the corresponding columns) are selected at random and the active zone heights in the selected column and its nearest neighbors are updated. Since it is necessary to keep a record of only the active zone height in each column and the algorithm is very simple, it is possible to carry out large scale simulations with modest computer memory requirements. In these simulations periodic boundary conditions are used in the x and y directions. In the x' direction a change in the lateral coordinate of L_x is accompanied by a height change of $L_x \tan\theta$ (truncated to the nearest integer).

III. GENERAL RESULTS

Figures 2 and 3 illustrate the structures obtained from simulations carried out with an angle of incidence or inclination angle (θ) of 80°. Figure 2 shows cross sections in the x-z plane [Fig. 1(a)] at two different heights. Similarly, Fig. 3 shows cross sections in the x-y plane (parallel to the inclined substrate) at four different distances from the substrate. These figures illustrate the characteristic "columnar" morphology which becomes more apparent further from the substrate. As the angle of incidence is increased towards 90° (grazing incidence) the mean density (fraction of occupied sites) decreases and the columnar morphology becomes more distinct. This is illustrated in Fig. 4 which shows cross sections in the x-y plane for simulations carried out with an angle of incidence of 87.5°.

At large angles of incidence the morphology can be described in terms of an assembly of overlapping "scales" inclined at an angle (ϕ) of about 37.5° from the normal. In some of the simulations the sites in the initial active zone at time $t=0$ were given distinct labels. When one of these sites was selected and filled to represent the growth process each of the new active zone sites was given the same label as the active zone site that was filled to create the new active zone sites. In this way the deposit is divided into clusters (each having a different label) corresponding to the scales. Figure 5 shows two of the scales identified in this fashion for the cross section shown in Fig. 4(c). Each of the scales has a characteristic size (s, number of occupied sites) length (l), width (w), and thickness (δ). The lengths l, w, and δ are measured along the z', y, and x' directions, respectively, in Fig. 1(b). These lengths grow algebraically with increasing cluster or scale size (s).

$$l \sim s^{\nu_\parallel} , \tag{8a}$$

$$w \sim s^{\nu_y} , \tag{8b}$$

$$\delta \sim s^{\nu_x} . \tag{8c}$$

We note that compactness of the individual scales implies $lw\delta \sim s$ or [26]

$$\nu_\parallel + \nu_x + \nu_y = 1 . \tag{9}$$

Figure 6 shows the cluster size distributions (N_s where $N_s \delta s$ is the number of clusters containing s to $s+\delta s$ sites). Here $\ln(s^{1.5}N_s)$ has been plotted against $\ln(s)$ so that a horizontal line corresponds to a power-law size distribution

$$N_s \sim s^{-\tau} \tag{10}$$

with a size distribution exponent (τ) of 1.5. In general, this exponent satisfies the relation [26]

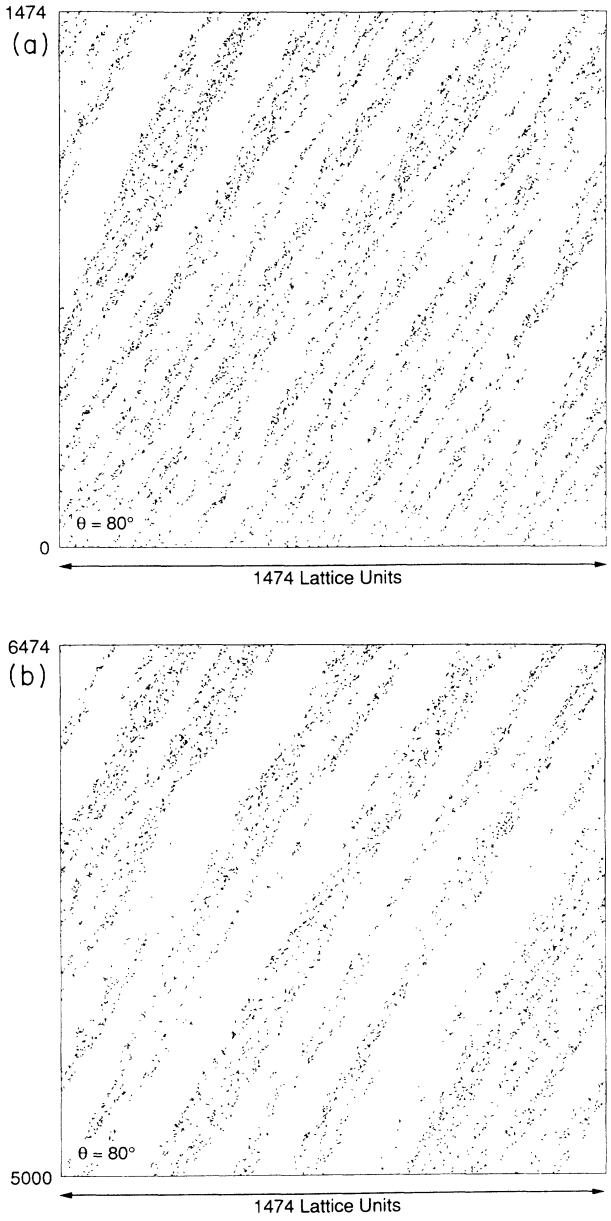

FIG. 2. Cross section through a deposit grown with an angle of incidence of 80°. The cross section is a plane that includes the normal to the substrate and the direction of incidence. (a) shows part of the cross section adjacent to the substrate and (b) shows part of the same cross section farther from the substrate.

$$\tau = 2 - \nu_{\parallel} . \tag{11}$$

Figure 6(a) shows the size distributions obtained from simulations carried out with several different values for the angle of incidence. These results were obtained from simulations carried out using lattices of size 1024×1024. Each simulation was carried out until a time of $t = 500$ had been reached (i.e., about 5×10^8 sites had been deposited) and the results from 5–10 simulations were averaged for each value of θ. Figure 6 shows that the size distribution exponent has a value very close to 1.5 for $\theta = 87.5°$ (i.e., near-grazing incidence).

Similarly, Fig. 6(b) shows the dependence of $\ln(s^{-1/3}w)$ on $\ln(s)$ obtained from the same simulations. Here w is the maximum cluster width in the y direction. Figure 6(b) indicates that for $\theta = 87.5°$ (near to grazing incidence) the exponent ν_y has a value of about 1/3. Figures 6(a) and 6(b) also indicate that the exponents τ and ν_y appear to change continuously as the angle of incidence is changed. These exponents change very little for angles of incidence near to 0° or 90° with the largest changes occurring at relatively large angles of incidence. Similar changes were observed in the effective values of $\nu_{\parallel}$ and ν_x. A similar apparently continuous change of the

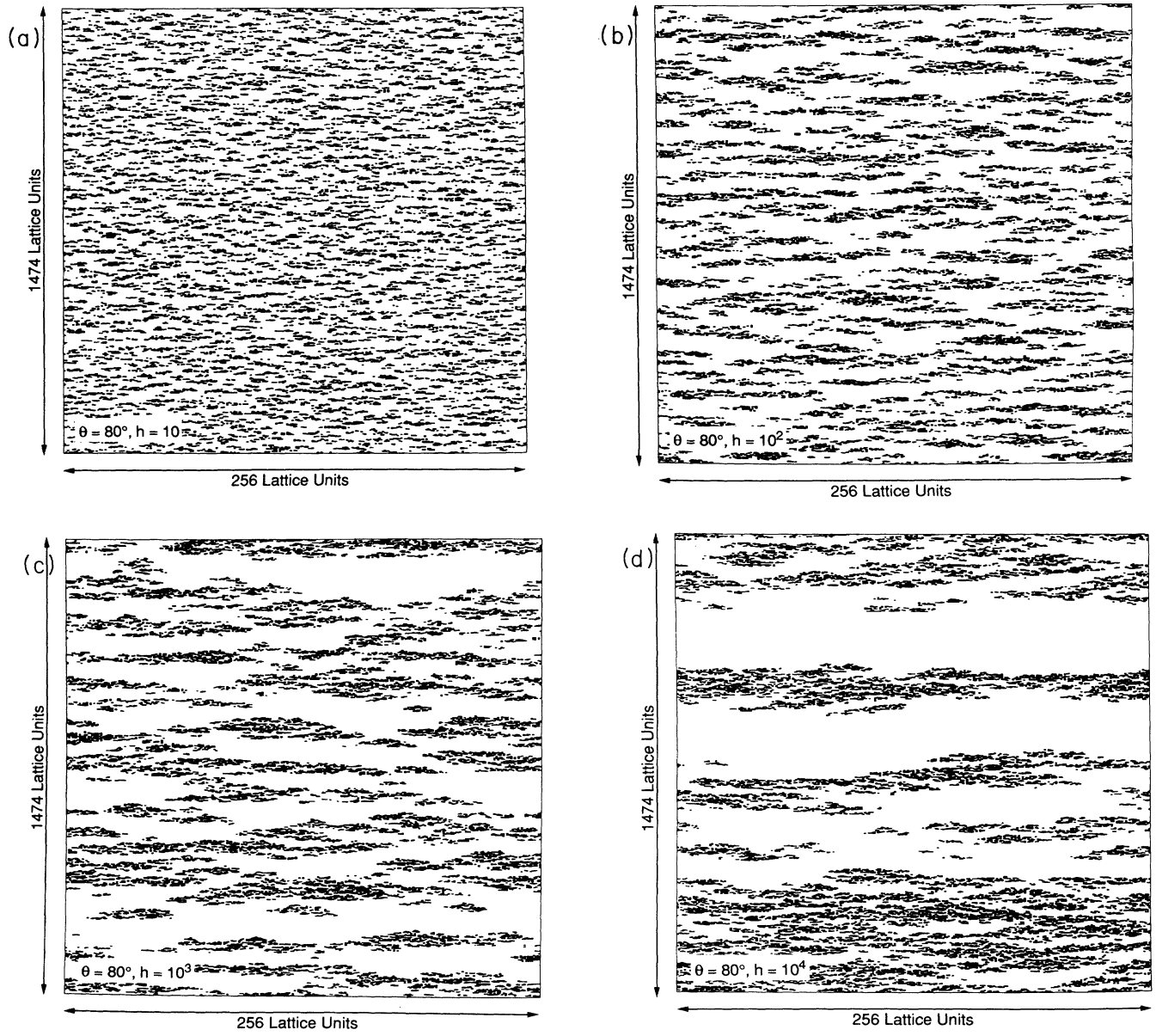

FIG. 3. Cross sections through a deposit generated with an angle of incidence of 80°. The cross sections are along planes parallel to the inclined substrate. The simulation was carried out in a column of size 256×256 ($x' \times y$) lattice units. The length in the x direction is $256/\cos(\theta)$. (a), (b), (c), and (d) show cross sections at heights (h) of 10, 100, 1000, and 10^4 lattice units where the height is the distance from the plane of cross section to the substrate.

exponents describing the columnar morphology was found in earlier work with the corresponding (square lattice) $(1+1)$-dimensional model [21,22]. This behavior has not yet been explained theoretically. The effective values for the exponents ν_x, ν_y, $\nu_\parallel$, and τ obtained from these and other simulations are shown in Table I together with the results obtained earlier [26] at normal incidence.

The number of clusters or scales $N(t)$ that survive to a time of t or greater was also measured. The simulation results indicate that

$$N(t)\sim t^{-\tau_t} \tag{12}$$

in the limit $t\to\infty$. This indicates that the number of clusters reaching a height h or greater from the substrate is given by

$$N(h)\sim h^{-\tau_h} \tag{13}$$

where the exponents τ_t and τ_h are equal. The values obtained for this exponent are also given in Table I. The scaling relations (8a), (10), and (13) imply that

$$\tau_h=\frac{\tau-1}{\nu_\parallel}\ . \tag{14}$$

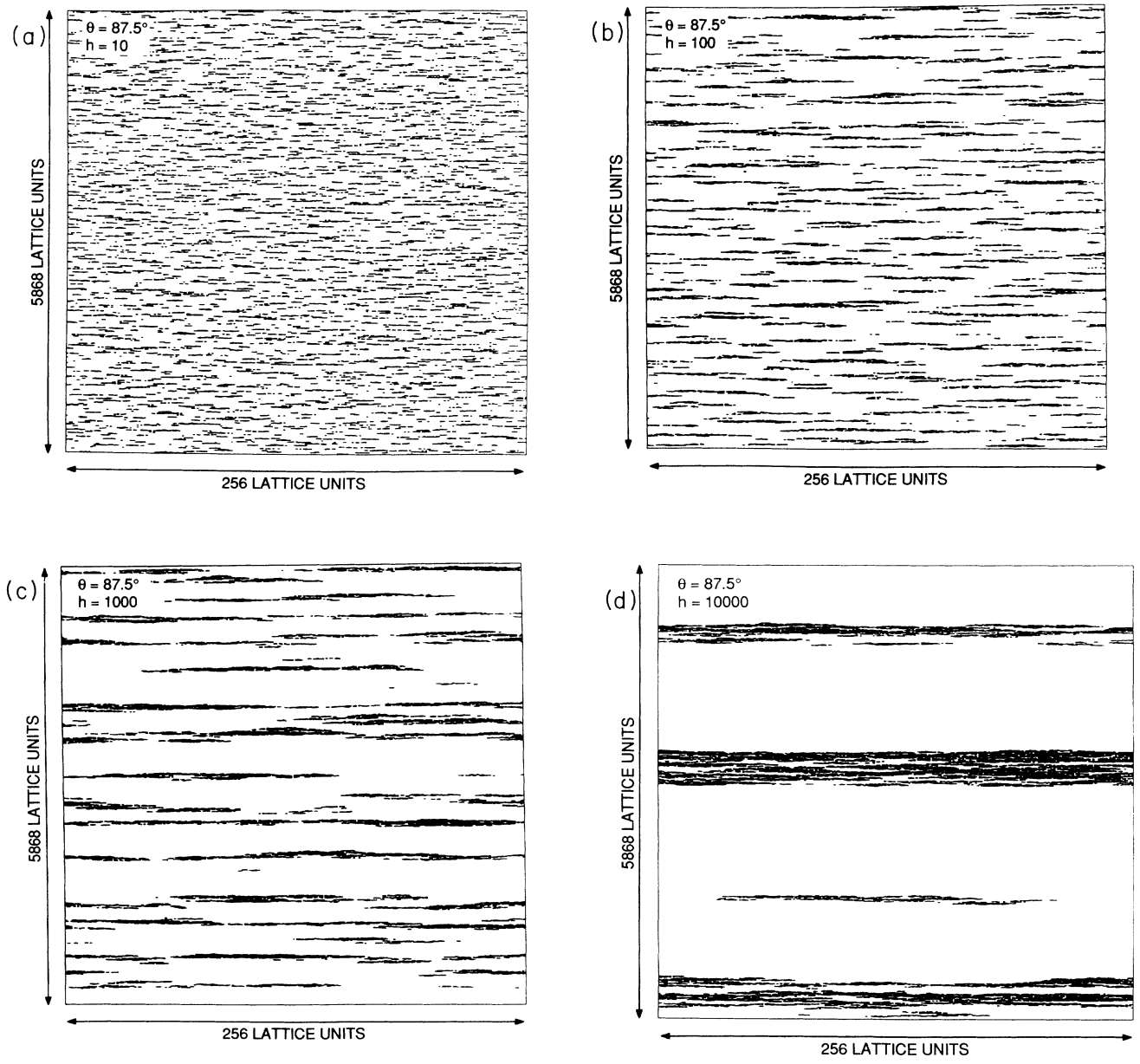

FIG. 4. Cross sections (parallel to the substrate) through deposits grown with a near-grazing angle of incidence of 87.5°. (a), (b), (c), and (d) show cross sections at heights of 10, 100, 1000, and 10^4 lattice units.

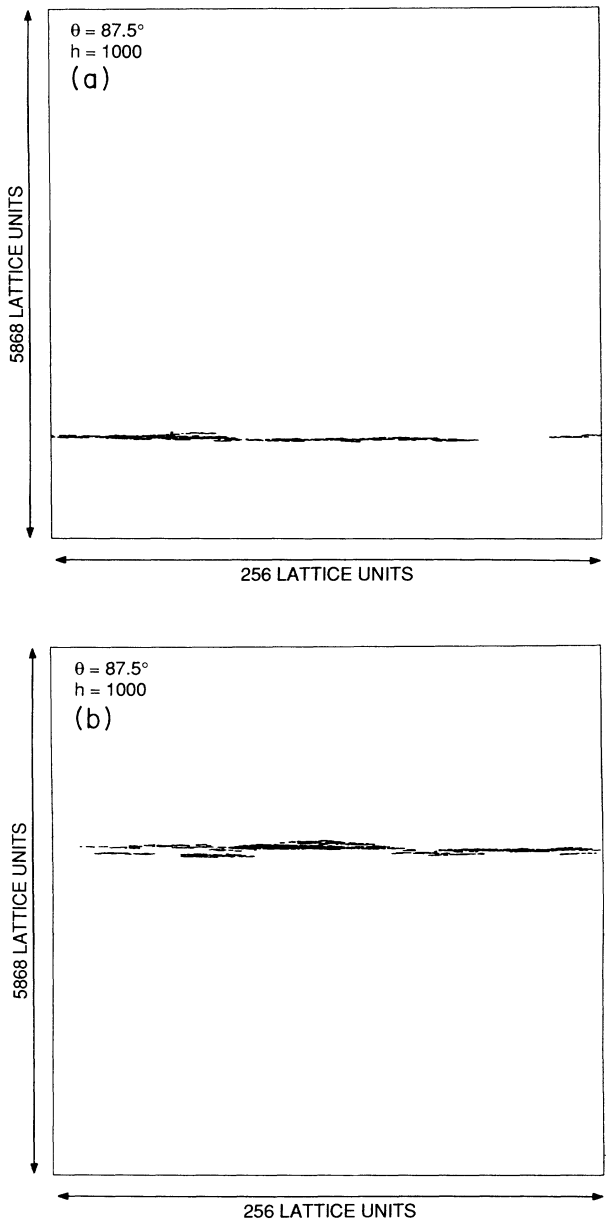

FIG. 5. Cross sections (parallel to the substrate) through individual clusters at a height of 1000 lattice units. These cross sections correspond to that shown in Fig. 4(c).

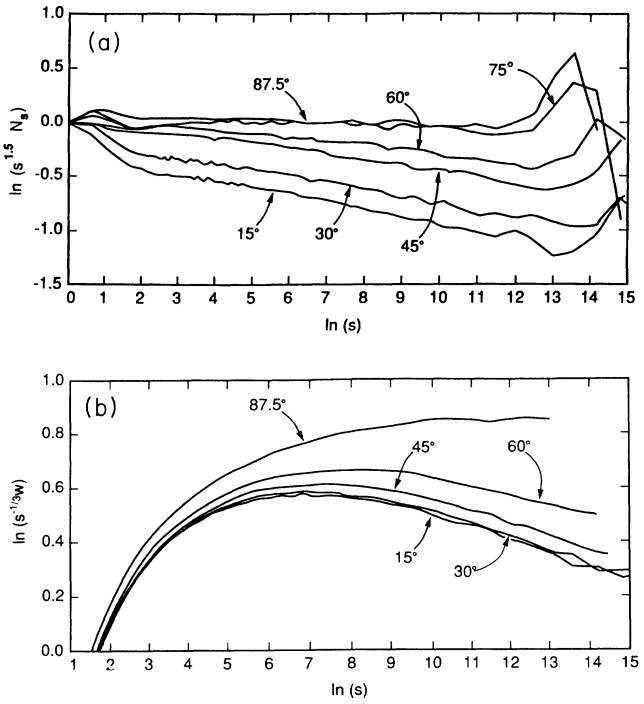

FIG. 6. (a) shows cluster size distributions (N_s) obtained from simulations carried out using five angles of incidence. (b) shows the dependence of the mean cluster widths (w) on the cluster size (s). The data have been plotted so that a horizontal curve corresponds to a size distribution exponent τ of 3/2 in (a) or width exponent ν_y of 1/3 in (b).

IV. SCALING ANALYSIS

For large angles of incidence large steps are found in the active zone. These steps occur at the growing edges of the overlapping clusters or scales. Figure 7 shows the location of these steps measured in the x'-y plane [Fig. 1(b)] for a simulation carried out with an angle of incidence of 87.5° on a lattice of size 512×512. Figure 7(a) shows the location of all those active zone sites for which the z' coordinate is higher than the height of the active zone in one or more of its nearest-neighbor columns by at least 100 lattice units. Similarly, Fig. 7(b) shows the location of those columns for which $z'_a(i,j) > z'_a(i-1,j)+100$

TABLE I. Exponents describing the cluster morphology obtained from (2+1)-dimensional cubic lattice model simulations of ballistic deposition.

Angle of incidence	ν_x	ν_y	$\nu_{\parallel}$	τ	τ_h
0°	0.283±0.002	0.283±0.002	0.452±0.002	1.566±0.002	
15°				1.570±0.004	
30°			0.467±0.001	1.568±0.005	1.283±0.001
45°				1.557±0.003	1.269±0.001
60°			0.488±0.001	1.545±0.003	1.200±0.001
70°		0.337±0.001	0.498±0.001	1.525±0.004	1.152±0.001
80°		0.345±0.001	0.515±0.008	1.515±0.008	1.050±0.001
87.5°		0.345±0.001	0.504±0.002	1.504±0.002	1.031±0.001

and Fig. 7(c) shows the location of those columns for which $z'_a(i,j) > z'_a(i,j-1)+100$ or $z'_a(i,j) > z'_a(i,j+1)+100$ where $z'_a(i,j)$ is the z' coordinate of the active zone in the column at position $x'=i$ and $y=j$. These figures locate the ragged edges of the clusters which define the deposit morphology. It is apparent from Fig. 7 that although the clusters or scales are quite thin, they are essentially opaque.

We have shown previously [25] that for very large angles of incidence (almost grazing incidence) the size distribution of the large steps can be represented by the simple scaling form

$$N_\delta(t) \sim \delta^{-\mu} f(\delta/t^\beta) , \tag{15}$$

where the exponents μ and β have values of 2 and 1/3, respectively. $N_\delta(t)$ is the number of steps of size δ at time t.

The structure displayed in Fig. 7 is the starting point of the scaling analysis presented in Ref. [25]. There we pointed out that the *cluster edges* evolve according to a growth process reminiscent of the two-dimensional Eden model [15,19], and hence their fluctuations can be described by the KPZ equation [20] for a one-dimensional moving interface. As in (1+1)-dimensional ballistic deposition at near-grazing incidence [22], these fluctuations drive the coarsening of the columnar structure by allowing some scales to grow ahead of others and thereby shadowing them. However, as long as a part of the edge of a scale is exposed to the particle beam, its growth is not halted by the presence of other scales. As a consequence, the collective properties of the deposit structure

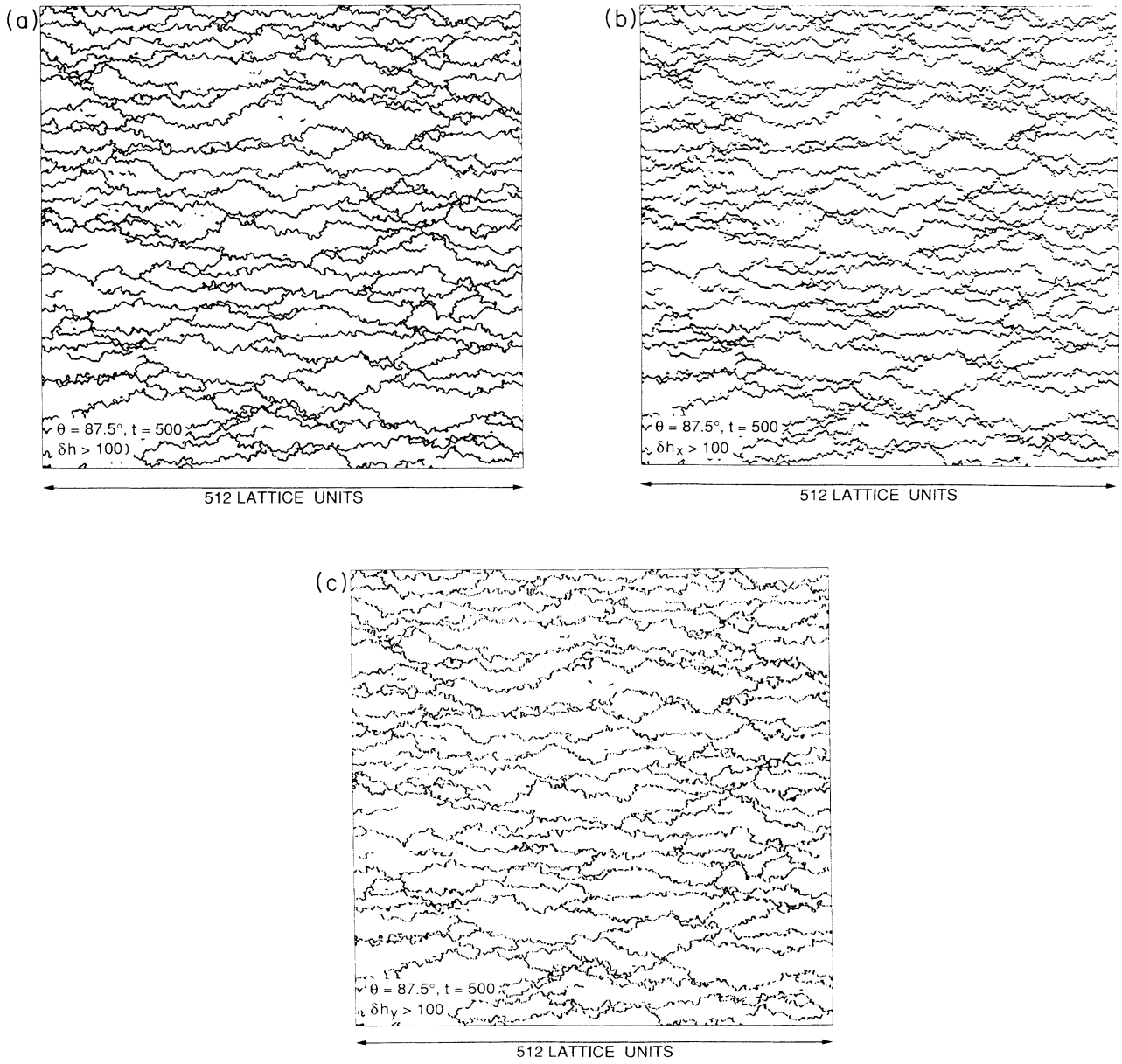

FIG. 7. Location of the large steps in the upper surface of a deposit generated using an angle of incidence of 87.5°.

can be deduced from the fluctuations of a *single edge*. In particular, the size and shape of the exposed parts of the scales visible in Fig. 7 (the "domains") is determined by the size and shape of the typical bumps present in a one-dimensional interface that has been growing for a time t. Hence the surface correlation lengths ξ_x and ξ_y can be identified with the correlation lengths of the one-dimensional interface, $\xi_x \sim \xi_{\perp}^{(1+1)}$ and $\xi_y \sim \xi_{\parallel}^{(1+1)}$ and the values

$$\sigma_x = \beta^{(1+1)} = 1/3 \ , \qquad \sigma_y = 1/z^{(1+1)} = 2/3 \tag{16}$$

follow from the exact solution [20] of the (1+1)-dimensional KPZ equation.

The large steps in the active zone are of the order of the typical distance between scale edges in the x' direction, and, therefore, the exponent β in the step size distribution (15) is given by $\beta = \sigma_x = \beta^{(1+1)} = 1/3$.

It is also clear from Fig. 7 that the correlation lengths ξ_x and ξ_y determine the width and thickness of the scales which are still exposed at time t. The mass of these scales is given by $s \sim l^{1/\nu_{\parallel}} \sim t^{1/\nu_{\parallel}}$ and consequently, using Eqs. (6) and (8) we obtain [25]

$$\nu_x = \nu_{\parallel} \sigma_x \ , \qquad \nu_y = \nu_{\parallel} \sigma_y \ . \tag{17}$$

Together with (9), (11), and (14) this fully determines the cluster exponents to be [25]

$$\nu_x = 1/6, \quad \nu_y = 1/3, \quad \nu_{\parallel} = 1/2 \ , \qquad \tau = 3/2, \quad \tau_h = 1 \tag{18}$$

in good agreement with the simulation results at near-grazing incidence. We mention that the relations (17) also hold for normal incidence ballistic deposition, however, with σ_x and σ_y replaced by $1/z^{(2+1)}$, the inverse of the (2+1)-dimensional KPZ dynamic exponent [22].

V. CROSSOVER REGIMES IN FINITE SYSTEMS

Because of the variety of characteristic lengths (ξ_x, ξ_y, L_x, and L_y) associated with three-dimensional grazing incidence ballistic deposition, a variety of scaling regimes and crossover phenomena can be observed. Two time scales can be defined by equating the correlation lengths ξ_x and ξ_y to the corresponding substrate dimensions,

$$T_x \sim L_x^{1/\sigma_x} = L_x^3 \ , \qquad T_y \sim L_y^{1/\sigma_y} = L_y^{3/2} \ . \tag{19}$$

We distinguish three cases for the late time behavior, according to whether (I) $T_x \ll T_y$, (II) $T_y \ll T_x$, or (III) $T_x \sim T_y$. The early time behavior of the overall surface width

$$\xi(L,t)^2 = \frac{1}{L_x L_y} \sum_{i=1}^{L_x} \sum_{j=1}^{L_y} (h_{i,j} - \bar{h})^2 \tag{20}$$

is dominated by the large steps in the active zone [25] and therefore $\xi \sim t^{\beta}$ with $\beta = 1/3$ for $t \ll T_{x,y}$. In case I this behavior changes when $t \sim T_x \sim L_x^3$. At that point only a single cluster is left in the system. The width $\xi \sim L_x$ and cannot grow any further. Thus this case is governed by a conventional scaling form [cf. Eq. (4)]

$$\xi(L_x,t) = L_x f(t/L_x^3) \tag{21}$$

with $f(x) \to$ const for $x \to \infty$ and $f(x) \sim x^{1/3}$ for $x \to 0$. The dynamic exponent for case I is $z = 1/\sigma_x = 3$. Note that once ξ has saturated, the further increase of the correlation length ξ_y is impeded by the finite extension of the system in the x direction, and the time scale $T_y \gg T_x$ becomes irrelevant.

In case II (which is the one of relevance for isotropic scaling, $L_x \sim L_y \sim L$) a first crossover occurs when $t \sim T_y \sim L_y^{3/2}$. At this time the leading edges of the advancing clusters span the lattice in the y direction and the deposition process becomes equivalent to (1+1)-dimensional ballistic deposition. In the grazing incidence limit this process can be mapped onto that of coalescing Brownian particles on a line [22] where the Brownian particles represent the motion of the cluster tips or leading edges in a moving coordinate system. Values of 1.330 ± 0.003, 0.502 ± 0.003, and 0.674 ± 0.001 were obtained for the exponents τ, τ_h, and $\nu_{\parallel}$ from simulations carried out using substrates of size $L_x \times L_y = (16\,384 \times 2)$ in the $\xi_y > L_y$ regime. The exponents are in good agreement with those predicted by the mapping onto the particle coalescence problem [22] ($\tau = 4/3$, $\tau_h = \frac{1}{2}$, $\nu_{\parallel} = 2/3$).

A series of simulations was carried out with an angle of incidence of 89° with a substrate length (L_x) of 4096 lattice units and widths (L_y) ranging from 2 to 64 lattice units. Figure 8(a) shows the time dependence of the surface roughness (ξ) in the form of plots of $\ln(\xi/t^{1/2})$ vs $\ln(t)$. The slope of approximately $-\frac{1}{6}$ for the larger values of L_y corresponds to a value of 1/3 for the exponent β. Figure 8 shows that the exponent β crosses over to a value of 1/2 (the characteristic value of the (1+1)-dimensional model [21]) at late times. The crossover is expected to occur when ξ_y grows to a length L_y so that it is natural to represent the results shown in Fig. 8(a) by the scaling form

$$\xi = L_y^{-\gamma} t^{1/2} f(t/L_y^{3/2}) \ . \tag{22}$$

In order to represent both the short- and long-time behavior the scaling function $f(x)$ in Eq. (22) must have the form $f(x) = x^{-1/6}$ for $x \ll 1$ and $f(x) =$ const for $x \gg 1$ and since the short-time behavior is independent of the length L_y it follows that the exponent γ must have a value of 1/4.

This is in agreement with a recent study [27] in which the long-time ($t \gg L^z$) behavior of a driven interface was derived from the KPZ equation [20]. For long times the interface diffuses like a rigid object, with a *center of mass fluctuation* $\xi_c \sim (Dt)^{1/2}$ where the diffusion coefficient scales as $L^{-1/2}$ in 1+1 dimension. To test these simple scaling ideas the dependence of $\ln(\xi L_y^{1/4} t^{-1/2})$ on $\ln(t/L_y^{3/2})$ is shown in Fig. 8(b) for the four larger values

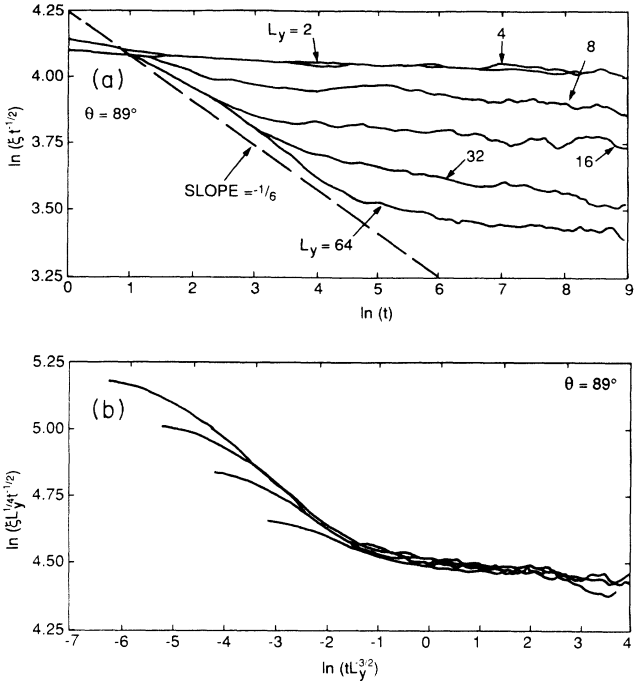

FIG. 8. Growth of the surface roughness (ξ) in narrow systems with an angle of incidence of 89°. (a) shows the dependence of $\ln(\xi t^{-1/2})$ on $\ln(t)$ for six different widths ($L_y = 2$, 4, 8, 16, 32, and 64). (b) shows how these curves can be scaled using the scaling form given in Eq. (22).

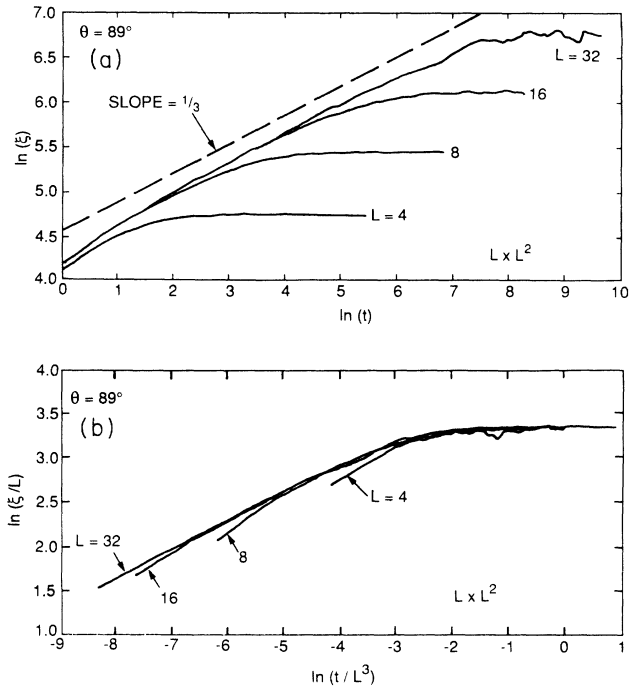

FIG. 9. Growth of the surface roughness (ξ) obtained from simulations carried out using systems of size $L_x = L$, $L_y = L^2$ with an angle of incidence of 89°. (a) shows the growth of ξ for four values of L. (b) shows that the dependence of ξ on L and t can be represented by Eq. (25).

of L_y ($L_y = 8, 16, 32, 64$). The data collapse supports the idea that the dependence of the surface width ξ on L_y and t can be represented by the scaling form given in Eq. (22).

A second crossover appears when the quasi-one-dimensional competition process between the coalescing cluster edges has eliminated all but one cluster. This occurs when

$$\xi \sim \frac{t^{1/2}}{L_y^{1/4}} \sim L_x \tag{23}$$

or

$$t \sim T_{\mathrm{II}} \sim L_x^2 L_y^{1/2} . \tag{24}$$

For $t \gg T_{\mathrm{II}}$ the surface width saturates. Hence the finite-size scaling behavior in case II is governed by *two different* dynamic time scales, and cannot be described by a single scaling form or a single dynamic exponent. We note that, in the isotropic case $L_x = L_y = L$, $T_{\mathrm{II}} \sim L^{5/2} \ll T_x$.

Finally in case III the two crossovers associated with T_x and T_y merge. This is illustrated in Fig. 9(a) where the growth of ξ is shown for simulations carried out using systems of size ($L_x \times L_y$) given by $L_x = L$ and $L_y = L^2$ ($L = 4, 8, 16, 32$). Figure 9(b) shows that the dependence of ξ on L and t can be represented quite well by the simple scaling form

$$\xi = L f(t/L^3) \tag{25}$$

with a dynamic exponent $z = 1/\sigma_x = 2/\sigma_y = 3$.

*Present address: Department of Physics, University of Oslo, P. O. Box 1048 Blindern, N-0316 Oslo, Norway.
†Address after November 1, 1992: IFF, Forschungszentrum Jülich, P. O. Box 1913, W-5170 Jülich, Germany.

[1] B. B. Mandelbrot, *The Fractal Geometry of Nature* (Freeman, New York, 1982).
[2] J. Krug and H. Spohn, in *Solids far from Equilibrium*, edited by C. Godrèche (Cambridge University Press, Cambridge, England, 1991).
[3] M. J. Vold, J. Colloid. Sci. **14**, 168 (1959).
[4] M. J. Vold, J. Phys. Chem. **63**, 1608 (1959).
[5] M. J. Vold, J. Phys. Chem. **64**, 1616 (1960).
[6] S. Kim, D. J. Henderson, and P. Chaudhari, Thin Solid Films **47**, 155 (1977).
[7] H. J. Leamy and A. G. Dirks, J. Appl. Phys. **49**, 3430 (1978).
[8] A. G. Dirks and H. J. Leamy, Thin Solid Films **47**, 219 (1977).
[9] H. J. Leamy, G. H. Gilmer, and A. G. Dirks, in *Current Topics in Materials Science*, edited by E. Kaldis (North-Holland, Amsterdam, 1980), Vol. 6.
[10] J. M. Niewenhuizen and H. B. Haanstra, Phillips Tech. Rev. **27**, 87 (1966).
[11] O. Geszti, L. Gosztola, and E. Seyfried, Thin Solid Films

136, L35 (1986).
[12] J. Jurusik and L. Zdanowicz, Thin Solid Films **144**, 241 (1986).
[13] M. J. Bloemer, J. L. Ferrell, M. C. Buncick, and R. J. Warmack, Phys. Rev. B **37**, 8015 (1988).
[14] T. Hashimoto, K. Okamoto, K. Hara, M. Kamiya, and H. Fujewara, Thin Solid Films **91**, 145 (1982).
[15] M. Eden, in *Proceedings of the 4th Berkeley Symposium on Mathematics, Statistics and Probability,* edited by F. Neyman (University of California Press, Berkeley, 1961), Vol. 4, p. 223.
[16] *Dynamics of Fractal Surfaces,* edited by F. Family and T. Vicsek (World Scientific, Singapore, 1991).
[17] B. B. Mandelbrot, Phys. Scr. **32**, 257 (1985).
[18] F. Family and T. Vicsek, J. Phys. A **18**, L75 (1985).
[19] R. Jullien and R. Botet, Phys. Rev. Lett. **54**, 2055 (1985).
[20] M. Kardar, G. Parisi, and Y.-C. Zhang, Phys. Rev. Lett. **56**, 889 (1986).
[21] P. Meakin, Phys. Rev. A **38**, 994 (1988).
[22] J. Krug and P. Meakin, Phys. Rev. A **40**, 2064 (1989).
[23] P. Meakin, P. Ramanlal, L. M. Sander, and R. C. Ball, Phys. Rev. A **34**, 5091 (1986).
[24] J. Krug, Phys. Rev. A **36**, 5465 (1987).
[25] P. Meakin and J. Krug, Europhys. Lett. **11**, 7 (1990).
[26] P. Meakin, J. Phys. A **20**, L1113 (1987).
[27] J. Krug, Phys. Rev. A **44**, 801 (1991).